

# Maximizing Electric Power through Spectral-Splitting Photovoltaic-Thermoelectric Hybrid System Integrated with Radiative Cooling

Jiangfeng Guo\* and Xiulan Huai

As zero-emission technologies, a daytime radiative cooling (RC) strategy developed recently, and photovoltaic (PV) and thermoelectric (TE) technologies have aroused great interest to reduce fossil fuel consumption and carbon emissions. How to integrate these state-of-the-art technologies to maximise clean electricity from the sun and space remains a huge challenge, and the limit efficiency is still unclear. In this study, a spectral-splitting PV-TE hybrid system integrated with RC is proposed to maximise clean electricity from the sun and space without any emissions. For the sun acting as a typical constant heat-flux heat source, the current thermoelectric theory overestimates the thermoelectric efficiency highly since the theory is based on constant temperature-difference conditions. A new theory based on heat-flux conditions is employed to achieve maximum thermoelectric efficiency. The PV-TE hybrid system with RC is superior to the conventional hybrid system, not only in terms of higher efficiency but also in its 24-h operation capacity. In a system with a single-junction cell, the total efficiency with 30 suns (39.4%) is higher than the theoretical PV efficiency at 500 suns (38.2%). In a hybrid system with four-junction cells, total efficiency is over 65% which is superior to most current photoelectric and thermal power systems.

## 1. Introduction

To tackle the challenges relating to environmental pollution and climate change, clean and renewable energy is increasing its penetration in the energy landscape, aiming at reducing the use of conventional fossil fuels.<sup>[1]</sup> Among all renewables, solar energy is the most important one thanks to its simple accessibility, cleanliness, and unlimited potential. Solar energy can be directly converted into electricity through photovoltaic (PV) cells without noise or moving components.<sup>[2]</sup> The efficiency limit of a conventional single-junction solar cell is around 33%, also known as Shockley–Queisser (S-Q) limit,<sup>[3]</sup> which is much lower than Landsberg (93%) and Carnot limits (95%),<sup>[4]</sup> since a large portion of the solar spectrum cannot be used in the photon-electricity conversion.

The unused portion of the solar spectrum dissipates as waste heat in PV cells, including the photon energy below/above the PV cell's bandgap energy ( $E_g$ ). It is

acknowledged that the PV efficiency decreases relatively by 4.5% and the ageing rate of PV cells doubles for an increase of 10 °C in the PV cell's temperature ( $T_{PV}$ ).<sup>[5]</sup> Therefore, enhancing spectrum utilization and reducing waste heat generation to fill the gap between S-Q and Carnot limits have attracted significant attention in recent decades, and various design strategies and concepts such as spectral-splitting (SS) technology and multi-junction (MJ) solar cells have been proposed.<sup>[6]</sup> The photons with energy below  $E_g$  can be split via SS and further exploited through other options to enhance the full-spectrum utilization. MJ solar cells, which consist of multiple stacked PV cells with different  $E_g$ , can absorb the appropriate band that matches the  $E_g$  of a specific cell, thereby enhancing the overall efficiency.<sup>[7]</sup>


Another way to improve the solar utilization efficiency of PV cells is to utilize the waste heat through a thermoelectric generator (TEG) to produce additional electricity. In a hybrid photovoltaic-thermoelectric (PV-TE) system, it is generally to direct the ultraviolet (UV) and visible bands of the solar spectrum to the PV cell, while the infrared (IR) band is directed to a heat absorber that acts as the hot side of TEG via concentrated SS.<sup>[8]</sup> Elsarrag et al.<sup>[9]</sup> conducted theoretical and experimental studies on a hybrid PV-TE system to address the feasibility of using such

J. Guo, X. Huai  
Institute of Engineering Thermophysics  
Chinese Academy of Sciences  
Beijing 100190, P. R. China  
E-mail: guojf@iet.cn; gjf1200@126.com

J. Guo  
Department of Chemical Engineering  
Imperial College London  
London SW7 2AZ, UK

J. Guo, X. Huai  
Nanjing Institute of Future Energy System  
Nanjing 211135, P.R. China

J. Guo, X. Huai  
School of Engineering Science  
University of Chinese Academy of Sciences  
Beijing 100049, P. R. China

 The ORCID identification number(s) for the author(s) of this article can be found under <https://doi.org/10.1002/advs.202206575>

© 2023 The Authors. Advanced Science published by Wiley-VCH GmbH. This is an open access article under the terms of the Creative Commons Attribution License, which permits use, distribution and reproduction in any medium, provided the original work is properly cited.

DOI: 10.1002/advs.202206575

systems in large-scale applications. Yin et al.<sup>[10]</sup> proposed an optimization method to maximize solar energy harvest for SS PV-TE systems, with results showing that there existed an optimal temperature distribution in the TE subsystem. The optimal cut-off wavelength was the maximum available wavelength of GaAs PV cell and was slightly affected by the convective heat transfer coefficient of the cooling system when the thermoelectric figure of merit was small, and the optimal cutoff wavelength decreased as the figure of merit increased. Alnajideen and Min<sup>[11]</sup> experimentally investigated a hybrid PV-TE system with SS strategy, and the results showed that the overall efficiency was increased by 6.3% due to the harvesting of IR spectrum using TEG, and a further increase in efficiency could be achieved using light concentration. Another commonly used method is to place TE modules directly underneath PV panels, with PV panels acting as the hot sides of TE modules. Khan et al.<sup>[12]</sup> performed an experimental study of such configurations, and the results showed that the  $T_{PV}$  could be decreased by 3 K, and consequently, the total output power was increased by 19% and the overall solar-to-electric efficiency was increased by 17% with respect to the bare PV panels. The TE modules that operated alone under solar irradiation conditions were also studied. Peak efficiencies of 4.6% and 7.4% could be achieved with solar irradiances of 1 and 211 kW m<sup>-2</sup>, respectively, as reported by Kraemer et al.<sup>[13]</sup>

Regardless of the structural form, a heat sink as the cold side is required in TEG, and various types are available. The common cooling methods include air cooling,<sup>[14]</sup> liquid cooling (e.g., water),<sup>[15]</sup> phase change materials,<sup>[16]</sup> etc., and the ambient is usually employed as the final cold source, resulting in a higher temperature in the cold side of TEG than the ambient temperature. As a clean and sustainable cooling technology that has been developed recently, daytime radiative cooling (RC) can emit heat to outer space with a temperature of 3 K through the “atmospheric window” (wavelength  $\lambda$  ranges from 8 to 13  $\mu\text{m}$ ) without any additional energy consumption, so as to achieve a lower cooling temperature than the ambient temperature.<sup>[17]</sup> Raman et al.<sup>[18]</sup> devised a photonic radiative cooler that could reflect >90% of the incident sunlight and emit heat through the atmospheric window, with experimental results showing that a temperature drop of 4.9 °C could be achieved relative to the ambient temperature at midday and demonstrating the feasibility of using RC as a clean cooling approach. Chen et al.<sup>[19]</sup> reported an average temperature drop of 37 °C relative to the ambient temperature was experimentally achieved after a 24-h day–night cycle, with a maximum temperature drop of 42 °C at midday.

PV panel has sufficient area to face the sky and is very suitable for the use of RC technology. Zhu et al.<sup>[20]</sup> integrated RC with a bare crystalline Si PV panel, demonstrating that the PV panel’s temperature could be reduced by 18.3 °C at 1 sun. Also, based on a crystalline Si cell, a PV system integrated with SS and RC was proposed by Gao et al.,<sup>[21]</sup> and the experimental results indicated that the panel’s temperature could be reduced by 23.2 °C when the wind speed was 3 m s<sup>-1</sup> and by 68.1 °C when there was no wind. Wang et al.<sup>[22]</sup> conducted multiple simulations and experiments to investigate the impact of radiative cooling on solar cells, they found RC performance varied significantly with changes in wind speed, heat load, and design, the temperature drop of 36 °C was observed in a sealed chamber relative to a system without RC. However, Li et al.<sup>[23]</sup> experimentally and theoretically investigated

the effect of RC on a commercial PV module, with results indicating that the temperature reduction and efficiency improvement were very slight, since the encapsulating layers (like glass cover) had high thermal emissivity. This issue could be partially addressed by optimized coating, Li et al.<sup>[24]</sup> reported that the temperature of an encapsulated PV module could be reduced by 5.7 °C, using a multilayer structure with strong reflectivity in UV and 1.3–1.8  $\mu\text{m}$  bands and high emissivity in the 4–25  $\mu\text{m}$  band. Besides, the actual effect of RC is affected by relative humidity, cloud cover, wind speed, latitude, etc.,<sup>[25]</sup> which remains to be further studied before its large-scale application. Fan et al.<sup>[26]</sup> presented a TEG-RC system, and the results showed that the power density of TEG could be increased by 53% relative to the scenario with regular blackbody emitters.

The theory of TEG operating at constant temperature-difference conditions has been established and has been widely adopted to estimate the TEG electrical power and efficiency.<sup>[27]</sup> The theory assumes that TEG works at a constant-temperature heat source, and its operating temperature difference does not change with the operating modes. However, the actual temperature difference varies with the operating modes (open circuit, closed circuit, short circuit, etc.), resulting in much lower efficiency than the theoretical efficiency. In addition, as a typical constant heat-flux condition, the temperature of the solar absorber that acts as the hot side of TEG varies with the properties of TEG. Therefore, how to accurately predict the maximum TE efficiency is crucial to exploit the potential of integrating TEG with PV panels in practical applications. Previous research mainly focuses on the applications of RC in PV panels or TE modules alone, high efficiency is hard to achieve, especially for stand-alone TE modules. Hybrid PV-TE systems achieve higher efficiency than stand-alone PV panels, while the capability of generating electricity during both daytime and nighttime without energy storage remains a challenge. Integrating RC with a hybrid PV-TE system at concentrated sunlight conditions, and the limit efficiency and operation mode remain unclear. In this study, we develop a methodology and a model to combine the state-of-the-art SS methodology, RC, and PV-TE hybrid technologies to maximize electricity generation from the sun and space without any emissions. The impacts of RC, concentration ratio, and material properties of PV panels on the maximum efficiency of the hybrid system are analyzed. This study provides insight into the SS, PV-TE, and RC technologies as well as useful guidance for the design and optimization of relevant components and systems.

## 2. Results

### 2.1. Single-Junction PV-TE Hybrid System

Photons with energy below  $E_g$  cannot be electrically utilized by PV cells and are thus converted to thermal energy. Similarly, for photons with energy over  $E_g$ , the excess energy that cannot be used by PV cells is also ultimately converted to thermal energy (i.e., the thermalization loss), as shown in **Figure 1a**. In both cases, this leads to the increasing operating temperature of PV cell ( $T_{PV}$ ), and decreasing PV efficiency ( $\eta_{PV}$ ) and lifespan. In a radiative cooler, the emissivity plays a crucial role, which can be classified as either narrowband cooling or broadband cooling as shown in **Figure 1b**. In a narrowband cooling, the high emis-

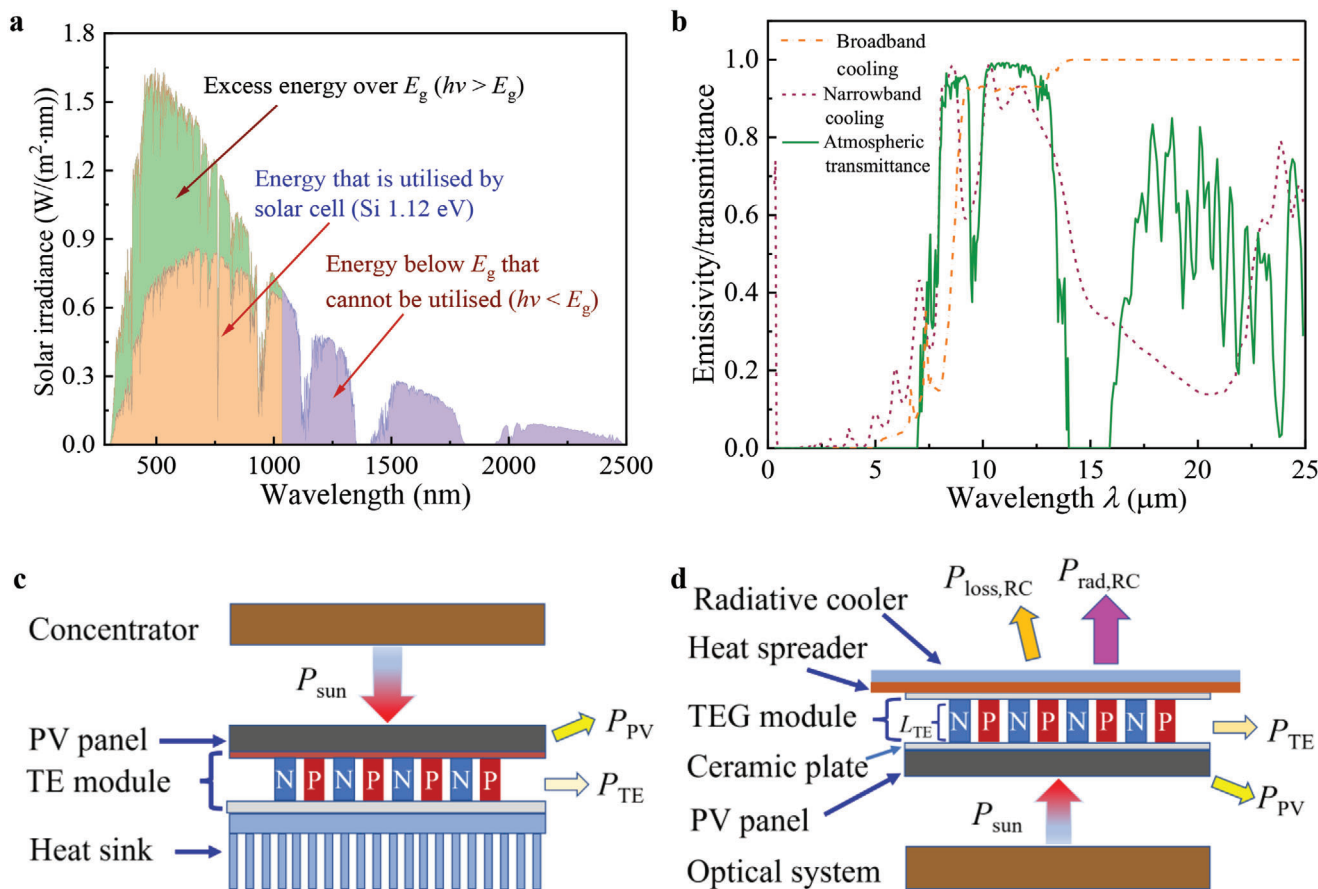


**Figure 1.** Solar spectrum, the emissivity of radiative cooler, PV-TE hybrid systems. a) The AM1.5 solar spectrum and the part of the spectrum irradiance that can be utilized by Si solar cell ( $E_g = 1.12$  eV). b) Emissivities of narrowband cooling in ref. [28] and broadband cooling in ref. [20] and atmospheric transmittance in ref. [31]. c) A hybrid PV-TE system with a heat sink. d) A hybrid PV-TE system with radiative cooling.

sivity should coincide with the “atmospheric window” as much as possible, while the emissivity in other bands ( $\lambda < 8 \mu\text{m}$  or  $\lambda > 13 \mu\text{m}$ ) should be as low as possible to achieve a temperature lower than the ambient temperature ( $T_a$ ). In broadband cooling, the emissivity should be zero in the solar spectrum and as high as possible in other bands as shown in Figure 1b (the emissivity in broadband cooling comes from ref. [20]), achieving a large cooling power with a temperature higher than  $T_a$ . A temperature lower than  $T_a$  is desired to benefit TEG, especially at night, so narrowband cooling is adopted in this study. The optimized multilayer structure of narrowband cooling adopted here was proposed in ref. [28], whose materials include  $\text{MgF}_2$ ,  $\text{TiO}_2$ ,  $\text{SiN}$ ,  $\text{SiO}_2$ , etc. The optical properties of these materials can be found in literature, and the emissivity of the multilayer structure could be obtained through the characteristics matrix method.<sup>[29]</sup> Multilayer films of these materials are commonly used for radiative cooling, and their effectiveness has been verified by experiments.<sup>[18,30]</sup>

In a conventional PV-TE hybrid system as shown in Figure 1c, a PV panel is placed on the top acting as the hot side of TEG, and a heat sink is placed at the bottom acting as the cold side of TEG. TE module consisting of numerous P-N thermocouples is placed in the middle, to generate electricity using the temperature difference between the solar panel and heat sink. Heat is dissipated

from the heat sink to the environment via convection and radiation, making the temperature of the heat sink higher than  $T_a$ . In this study, radiative cooling is used to replace the heat sink as the cold side of TEG to create a lower cold-side temperature than  $T_a$ . Radiative cooling needs to face the sky, so it is placed on the top as shown in Figure 1d. A solar panel is placed at the bottom as the hot side of TEG, while the TEG is placed in the middle to generate electricity using the temperature difference between the PV panel and RC. Compared with the system in Figure 1c, the light path in the system in Figure 1d is slightly more complicated, and it needs a reflector to direct sunlight to the solar panel from bottom to top. A similar light path scheme has been experimentally verified to have good performance in ref. [22].

The sunlight is AM1.5 spectral irradiation shown in Figure 1a, and the PV efficiency is calculated based on the method of detailed balance limit first introduced by Shockley and Queisser.<sup>[3]</sup> The  $T_{\text{PV}}$  is not fixed as in the classical analysis, but the temperature at which the PV cells reach heat balance with the surrounding components and environment (see Equation (17) in the Experimental Section) in this study. The PV efficiency can be written as

$$\eta_{\text{PV}} = \frac{P_{\text{PV}}}{\int_0^\infty C_t A_{\text{PV}} J_{\text{AM1.5}} d\lambda} \quad (1)$$

where  $P_{PV}$  denotes PV power,  $I_{AM1.5}$  refers to the AM1.5 standard spectral irradiance,<sup>[32]</sup>  $A_{PV}$  is the PV panel's area, and  $C_r$  is the concentration ratio which is defined as

$$C_r = \frac{A_{op}}{A_{PV}} \quad (2)$$

where  $A_{op}$  is the aperture area of the optical concentrator. Analogous to the concentration ratio, the cooling ratio ( $R_c$ ) is defined as the ratio of the equivalent area of the cooler (including the heat sink) to the area of the PV panel

$$R_c = \frac{A_{RC}}{A_{PV}} \quad (3)$$

where  $A_{RC}$  denotes the area of radiative cooler, and also denotes the area of the heat sink in Figure 1c for the convenience of comparison. When the temperature of radiative cooler ( $T_{RC}$ ) is higher than  $T_a$ , heat is dissipated to outer space and the surrounding environment via radiation and convection. When  $T_{RC}$  is lower than  $T_a$ , heat is dissipated to outer space via radiation, while the surrounding environment will act as a heat source. Detailed information about RC can be found in Section *Radiative Cooling* in the Experimental Section. TEG needs to connect an external load in practical applications, and the ratio of external load resistance to internal resistance can be written as

$$s = \frac{R_l}{R_i} \quad (4)$$

where  $R_l$  is the external load resistance and  $R_i$  denotes the internal resistance of TEG. This ratio  $s$  has an important impact on the performance of TEG in the constant heat-flux theory adopted in this study, which is to overcome the invalidation of the current constant temperature-difference theory, and the details will be discussed in the following sections. One structural parameter that has an important influence on the TE power is the ratio of cross-sectional area to the length in the TE module

$$AL = \frac{N_{TE} A_{TE}}{L_{TE}} \quad (5)$$

where  $N_{TE}$  is the number of P-N thermocouples,  $A_{TE}$  is the cross-sectional area of a thermocouple, and  $L_{TE}$  is the length of P-N thermocouples. For the convenience of comparison, the equivalent efficiency of TEG in a hybrid PV-TE system is defined as

$$\eta_{TE_{eq}} = \frac{P_{TE}}{\int_0^\infty C_r A_{PV} I_{AM1.5} d\lambda} \quad (6)$$

where  $P_{TE}$  is the TE power. Therefore, the total efficiency of the hybrid PV-TE-RC system can be written as

$$\eta_{PV+TE} = \frac{P_{PV} + P_{TE}}{\int_0^\infty C_r A_{PV} I_{AM1.5} d\lambda} \quad (7)$$

$$\eta_{tot} = \frac{P_{PV} + P_{TE} + P_{TE_n}}{\int_0^\infty C_r A_{PV} I_{AM1.5} d\lambda} \quad (8)$$

where  $P_{TE_n}$  denotes the TE power at night.

The temperature and efficiency as a function of bandgap energy in the two systems in Figure 1c,d, under the same conditions of  $T_a = 300$  K,  $s = 2$ ,  $E_g = 1.4$  eV,  $AL = 0.014$  m,  $h_c = 5$  W m<sup>-2</sup> K<sup>-1</sup> (convective heat transfer coefficient, representing the heat exchanged with the atmosphere via convection, can be reduced by windshield or vacuum significantly), are presented in **Figure 2**. The  $T_{PV}$  is 5.6 K lower in the PV-TE-RC system than in the PV-TE system in Figure 1c on average in the range of  $E_g$ , indicating the RC has better cooling effectiveness than the heat sink and the PV panel performs better in the PV-TE-RC system. The temperature of heat sink ( $T_{hs}$ ) in the PV-TE system in Figure 1c is 1.4 K (on average) higher than  $T_a$  over the range of  $E_g$ , while the  $T_{RC}$  in the system in Figure 1d is 12 K (on average) lower than  $T_a$  during daytime. Of note is that  $T_{RC}$  is 285.1 K which is nearly 15 K lower than  $T_a$  at night. The total efficiency of PV panel and TEG ( $\eta_{PV+TE}$ ) in the conventional system in Figure 1c (the maximal value is 33.1%) is increased by 4.4% relatively (on average) compared to  $\eta_{PV}$  over the range of  $E_g$ , while  $\eta_{PV+TE}$  in the PV-TE-RC system (maximal value is 33.8%) is increased by 9.3% relatively compared to  $\eta_{PV}$  on average. More importantly, TEG can also generate electricity at night in the PV-TE-RC system since  $T_{RC}$  is lower than  $T_a$ . Considering the electricity generation of PV panel, TEG at both daytime and nighttime, the total equivalent efficiency ( $\eta_{tot}$ ) of the PV-TE-RC hybrid system is increased by 11.8% relatively compared to  $\eta_{PV}$  on average, and the maximum value reaches 34.2%, which is higher than the S-Q limit ( $\approx 33\%$ ) and the  $\eta_{PV+TE}$  in the conventional PV-TE system (33.1%) under 1 sun.

In the PV-TE-RC system in Figure 1d,  $C_r$  and  $R_c$  represent the intensity of "hot source" and "cold source," and their influences on the efficiencies and TE power at night are demonstrated in Figure 2c,d. At  $R_c = 20$ , with an increment of  $C_r$ ,  $\eta_{PV}$  increases to a peak (33%) at  $C_r = 2$  and then decreases due to the increasing  $T_{PV}$ , while  $\eta_{TE_{eq}}$  monotonously increases from 0.8% at  $C_r = 1$  to 1.9% at  $C_r = 6$ .  $C_r$  has no impact on TE power at night, but the  $\eta_{TE_{eq}}$  decreases from 0.4% at  $C_r = 1$  to 0.06% at  $C_r = 6$ . Although increasing  $C_r$  is beneficial to TEG,  $\eta_{PV}$  dominates in the total efficiency ( $\eta_{tot}$ ), and  $\eta_{tot}$  reaches a peak (34.3%) at  $C_r = 3$  and then decreases quickly. Because the TE module placed above the PV panel is not conducive to heat dissipation, when the deterioration effect of rising  $T_{PV}$  on PV panel outweighs the benefit to TEG,  $\eta_{tot}$  will inevitably decline. At  $C_r = 5$ , with the increment of  $R_c$  from 5 to 30,  $\eta_{TE_{eq}}$  increases from 1.2% to 1.8%,  $\eta_{TE_{eq}}$  at night rises from 0.05% (65 W m<sup>-2</sup>) to 0.08% (114 W m<sup>-2</sup>), and  $\eta_{PV}$  rises from 32.2% to 32.5%, leading to the increase in  $\eta_{tot}$  from 33.5% to 34.3%. Clearly, the increasing  $R_c$  is very conducive to the PV-TE-RC system, especially to TEG, while the increasing  $C_r$  is not always good for the efficiency of the whole system.

## 2.2. Spectral-Splitting PV-TE System

With the increase of  $C_r$ ,  $T_{PV}$  increases remarkably, leading to the decreasing  $\eta_{tot}$  in the PV-TE-RC system in Figure 1d. Under high  $C_r$  conditions, it is necessary to separate the spectrum with photon energy lower than  $E_g$  for reduction of  $T_{PV}$  as well as full-spectrum utilization as shown in **Figure 3**. The methodology to harvest solar energy by splitting solar spectrum and directing each band to the matching convertor was proposed first by

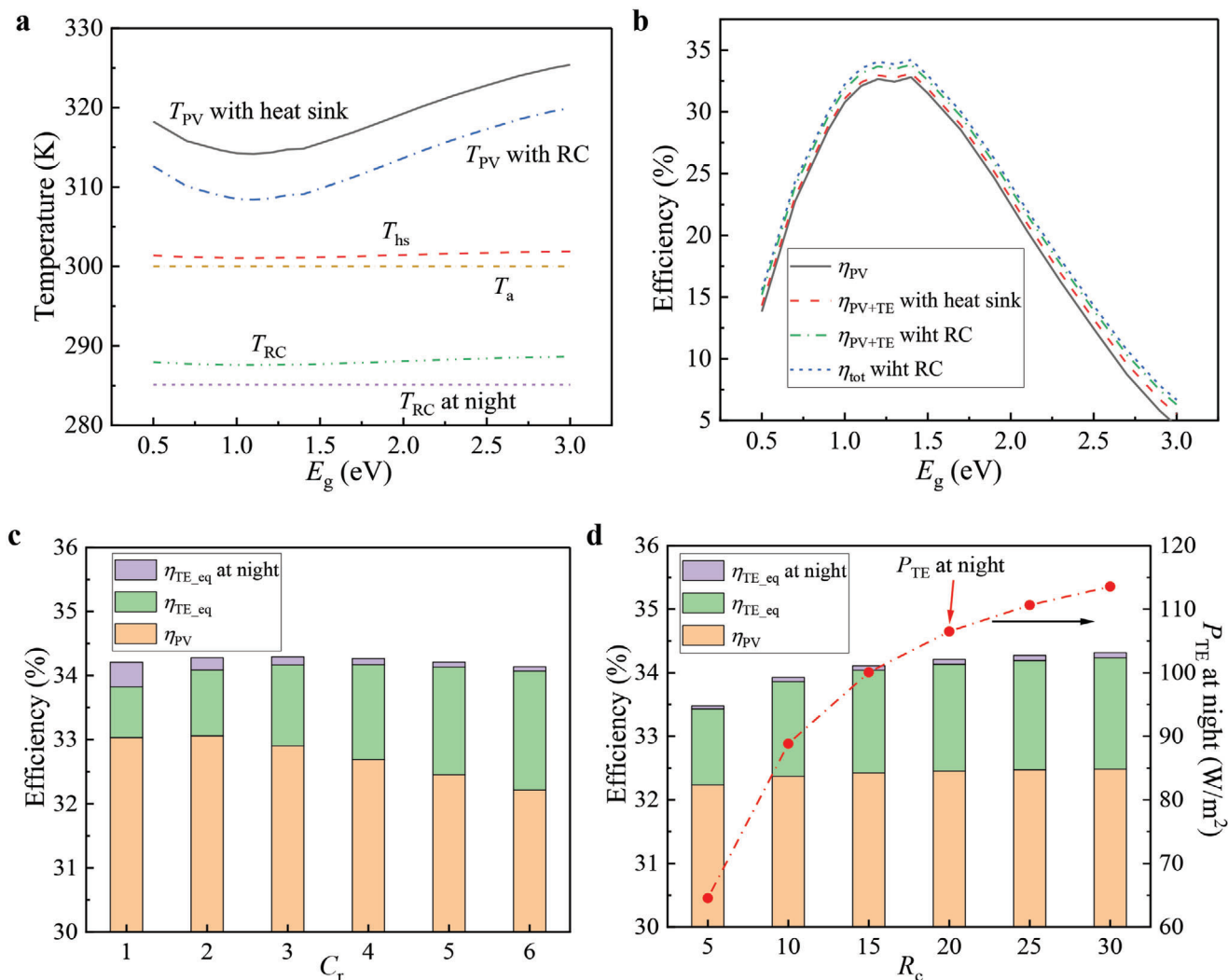


**Figure 2.** Temperature and efficiency in the hybrid systems in Figure 1. a) The temperature in the two PV-TE systems in Figure 1 as a function of bandgap energy at conditions of  $C_r = 1$  and  $R_c = 20$ . b) The efficiency in the two PV-TE systems in Figure 1 as a function of  $E_g$ , at conditions of  $C_r = 1$  and  $R_c = 20$ . c) Efficiencies in the PV-TE-RC system as a function of  $C_r$ , at  $R_c = 20$ . d) Efficiencies in the PV-TE-RC system and TE power at night as a function of  $R_c$  at  $C_r = 5$ . Other conditions:  $AL = 0.014$  m and  $s = 2$ .

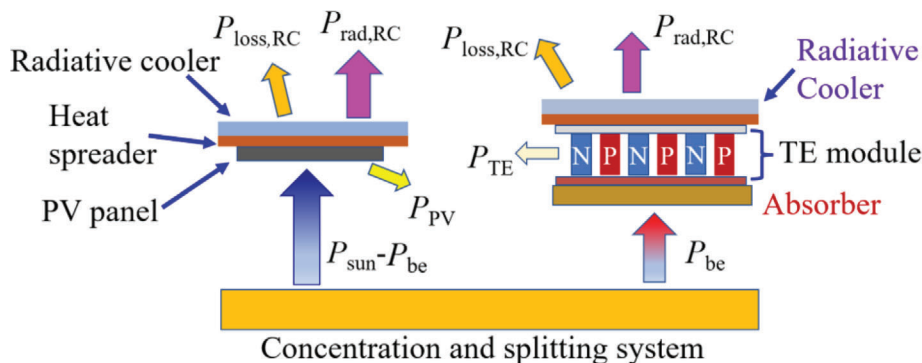


**Figure 3.** A concentrated spectral-splitting (SS) single-junction PV-TE-RC system. Photons with energy above  $E_g$  are directed to PV cell with matching  $E_g$ , the excess thermalization heat is dissipated through a radiative cooler placed above the PV panel. The separated spectrum is directed to a TE module that utilizes a radiative cooler to obtain a lower temperature than  $T_a$ .

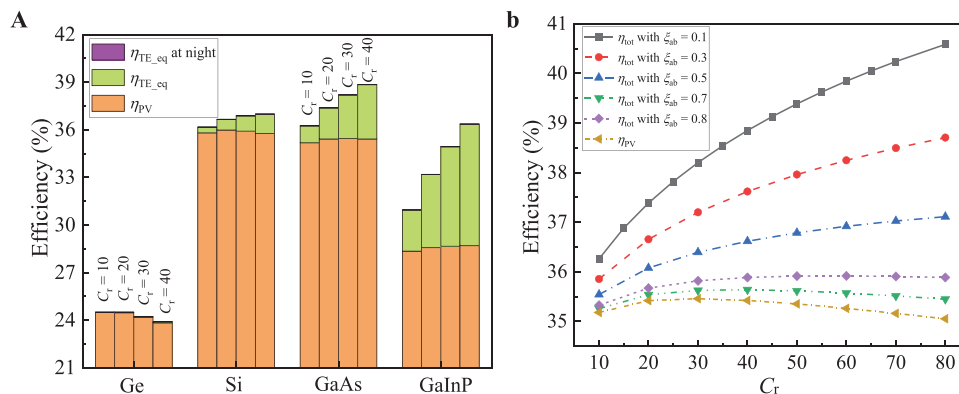


**Figure 4.** Efficiencies in the SS PV-TE-RC system as a function of  $C_r$  with various PV materials. a) Efficiencies as a function of  $C_r$  for different materials (Ge, Si, GaAs, and GaInP) at  $\xi_{ab} = 0.1$ . b) Efficiencies as a function of  $C_r$  with different heat loss coefficients of absorber at  $E_g = 1.42$  eV. Other conditions:  $R_c = 25$  and  $s = 2$ .

Jackson.<sup>[33]</sup> So far, various mechanisms and methods have been proposed for spectral-splitting of sunlight, such as refractive and diffractive methods, etc., and the details about these methods can be found in some excellent review papers.<sup>[34]</sup> The photons with energy above  $E_g$  are directed to PV panel with matching  $E_g$ , and the thermalization heat in the PV panel is dissipated through a radiative cooler placed above the PV panel, to avoid  $T_{PV}$  being too high under high  $C_r$ , and  $T_{PV}$  is restricted to be less than 373 K in this study. The separated photons with energy below  $E_g$  are directed to the absorber, whose temperature ( $T_{ab}$ ) can be very high (>400 °C) under high  $C_r$ , there are many ways to use the high-temperature absorber for power generation, such as TEG, thermal power generation, etc. Among them, TEG is one of the most convenient and environmentally friendly power generation methods with the lowest maintenance cost, so TEG is selected here. To further improve the efficiency of TEG, a radiative cooler is used as the cold side to obtain a lower temperature than  $T_a$  as shown in Figure 3.

According to the current thermoelectric theory under constant temperature-difference conditions, the maximum conversion efficiency can be obtained by<sup>[35]</sup>

$$\eta_{TE,max} = \left(1 - \frac{T_c}{T_h}\right) \frac{\sqrt{1+ZT} - 1}{\sqrt{1+ZT} + T_c/T_h} \quad (9)$$

with

$$s_{opt} = \sqrt{1+ZT} \quad (10)$$

where  $T_h$  and  $T_c$  denote the temperatures on the hot and cold sides of TEG,  $Z$  is figure-of-merit, and  $ZT$  denotes dimensionless figure-of-merit, which can be written as

$$ZT = \frac{\alpha^2}{\rho\lambda} T \quad (11)$$

where  $\alpha$  denotes Seebeck coefficient,  $\rho$  is electrical resistivity,  $\lambda$  denotes thermal conductivity, and  $T$  is the absolute temperature of the TE module that is often estimated to be  $(T_h+T_c)/2$ .

Of note is that Equation (9) is assumed that temperature difference ( $\Delta T$ ) across TEG is constant (i.e., constant-temperature heat

source,  $T_h$ ), and the ratio  $s$  has no effect on  $\Delta T$ . However,  $s$  has an important influence on the temperature difference across TEG, and the heat source (solar absorber) in the system in Figure 3 can be regarded as a constant heat-flux heat source rather than a constant-temperature heat source, making Equation (9) invalid. To address the issue in the current TE theory, a newly developed theory based on constant heat-flux conditions is adopted here,<sup>[36]</sup> the details about this new theory are presented in Section *Thermoelectric Efficiency under Constant Heat-Flux Conditions* in the Experimental Section. Based on the commonly used PV materials Ge ( $E_g = 0.66$  eV), Si ( $E_g = 1.12$  eV), GaAs ( $E_g = 1.42$  eV), and GaInP ( $E_g = 1.81$  eV), the efficiencies in the system in Figure 3 as a function of  $C_r$  are presented in Figure 4, at conditions of  $R_c = 25$ ,  $\xi_{ab} = 0.1$  (heat loss coefficient of absorber), and  $s = 2$ . As  $C_r$  increases from 10 to 40,  $\eta_{PV}$  decreases from 24.5% to 23.8% for Ge, reaches a peak of 36% at  $C_r = 20$  for Si, reaches a peak of 35.5% at  $C_r = 30$  for GaAs, and increases from 28.4% to 28.7% for GaInP. Figure 2c indicates that  $\eta_{PV}$  increases and then decreases as  $C_r$  increases, thus the optimal  $C_r$  at which  $\eta_{PV}$  reaches maximum increases as the material's  $E_g$  increases in Figure 4a.  $\eta_{TE,eq}$  increases as  $C_r$  rises, and grows greatly as the material's  $E_g$  increases, since the separated spectrum with photon energy below  $E_g$  increases as the material's  $E_g$  increases. For example,  $\eta_{TE,eq}$  is 0.04% for Ge on average over the range of  $C_r$  from 10 to 40, while is 5% for GaInP on average which increases more than 100-fold. This indicates that the selection of suitable PV material is crucial to this SS PV-TE-RC system. Although the Si PV panel has the highest  $\eta_{PV}$  among the four materials, the system including GaAs PV panel has the highest  $\eta_{tot}$  which is 37.7% on average over the range of  $C_r$  from 10 to 40. The absolute difference of  $\eta_{tot}$  between the systems including Si PV panel and GaAs PV panel increases as  $C_r$  increases, from 0.1% at  $C_r = 10$  to 1.9% at  $C_r = 40$ . The  $\eta_{TE,eq}$  at night becomes very small under high  $C_r$ , whose mean value is 0.01% over the range of  $C_r$  from 10 to 40. The  $\eta_{TE,eq}$  is very small in the system including Ge PV panel,  $\eta_{tot}$  is almost the same with  $\eta_{PV}$  and decreases as  $C_r$  grows due to increasing  $T_{PV}$ . However,  $\eta_{tot}$  increases as  $C_r$  grows for the other three PV materials, since the proportion of TE power increases.

To further analyze the tendency of  $\eta_{tot}$ , the effect of the heat loss coefficient of absorber ( $\xi_{ab}$ ) on  $\eta_{tot}$  is presented in Figure 4b, at  $R_c = 25$  and  $E_g = 1.42$  eV.  $\eta_{PV}$  increases to a peak of 35.5% at  $C_r$

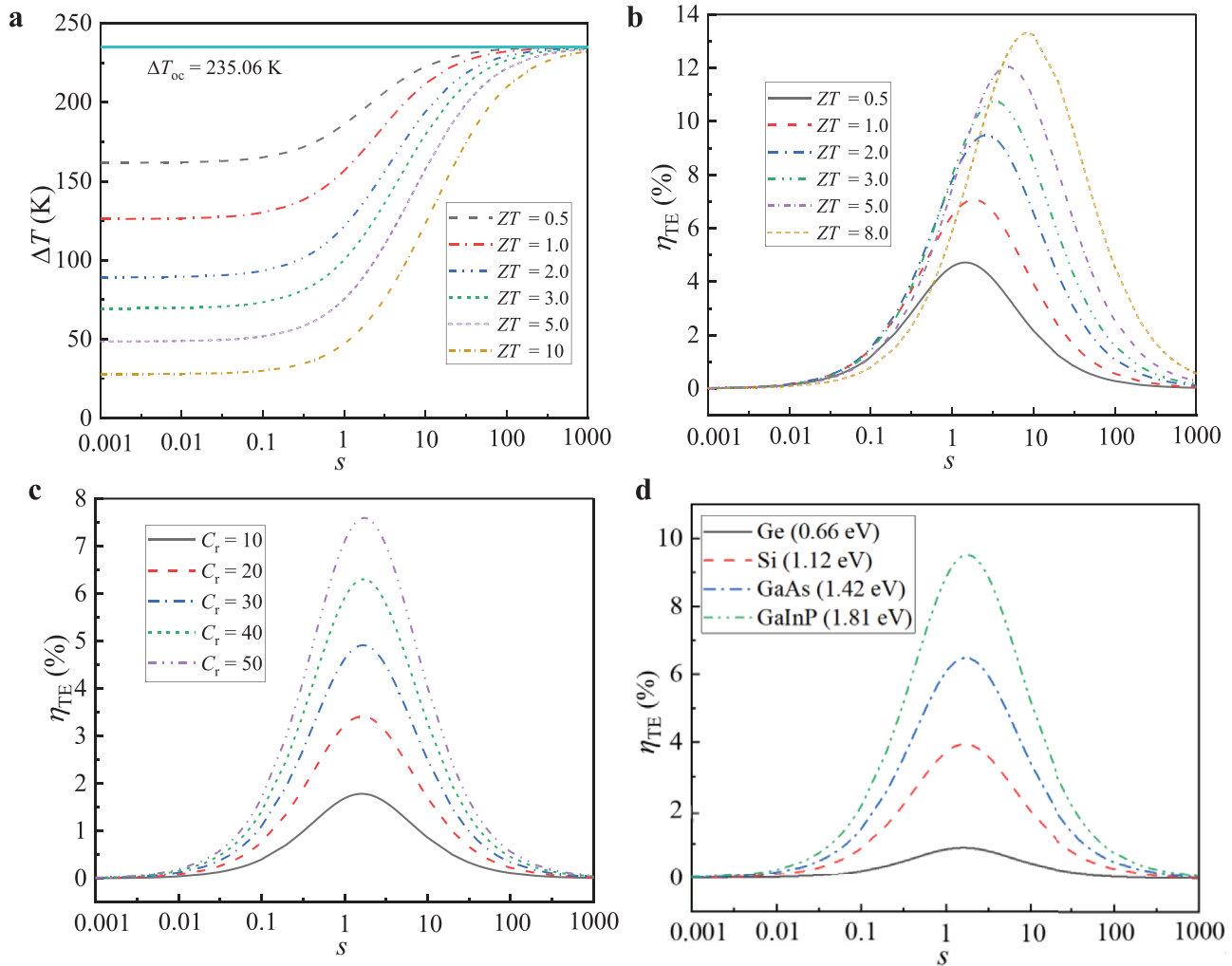


**Figure 5.** Temperature difference and TE efficiency as a function of  $s$  under various conditions in constant heat-flux theory. a) Temperature difference of TEG in a closed circuit as a function of  $s$  with various  $ZT$ , at  $C_r = 40$  and  $E_g = 1.4$  eV. b) TE efficiency as a function of  $s$  with various  $ZT$ , at  $C_r = 40$  and  $E_g = 1.4$  eV. c) TE efficiency as a function of  $s$  with various  $C_r$ , at  $Z = 2 \times 10^{-3} \text{ K}^{-1}$  and  $E_g = 1.4$  eV. d) TE efficiency as a function of  $s$  with various PV materials, at  $C_r = 40$  and  $Z = 2 \times 10^{-3} \text{ K}^{-1}$ . Other conditions:  $T_{c,oc} = 285.4 \text{ K}$  and  $\xi_{ab} = 0.1$ .

$= 30$ , and then decreases.  $\eta_{tot}$  also increases and then decreases in the cases of  $\xi_{ab} = 0.8$  and  $0.7$ , while the  $C_r$  corresponding to the maximal  $\eta_{tot}$  becomes higher as  $\xi_{ab}$  becomes lower, which is 40 at  $\xi_{ab} = 0.8$  and 60 at  $\xi_{ab} = 0.7$ . The decreasing  $\xi_{ab}$  means the increasing heat flux across TEG, leading to increasing  $\eta_{TE,eq}$ . Therefore,  $\eta_{tot}$  increases monotonously without a peak when  $\xi_{ab}$  is 0.5 or lower in the range of  $C_r$  from 10 to 80. In the range of  $C_r$  from 10 to 80, a 10% relative increment of  $\eta_{tot}$  is achieved (on average) compared to  $\eta_{PV}$  at  $\xi_{ab} = 0.1$ , even when half of the absorbed heat is lost (i.e.,  $\xi_{ab} = 0.5$ ),  $\eta_{tot}$  is still increased by 3.6% relatively on average. Various measures can be taken to reduce heat loss, such as placing the absorber in a vacuum environment to reduce convective heat loss, and increasing absorptivity in the solar spectrum and reducing emissivity in the emitted spectrum through suitable coating, etc. There are no moving parts or working mediums in the PV-TE-RC system, so it is easy to place this system in a closed or vacuum environment to reduce  $h_c$  and  $\xi_{ab}$ .

### 2.3. Thermoelectric Conversion Efficiency in Solar Energy

The theoretical efficiency of PV cells has been widely studied, while the TE theoretical efficiency under solar irradiance conditions is still misunderstood, which is one of the keys in the PV-TE-RC system. The presence of Peltier heat leads to a lower temperature difference ( $\Delta T$ ) across TEG in a closed circuit than in an open circuit, so the practical efficiency will be highly over-estimated using the constant  $\Delta T$  theory (i.e., Equation (9)).<sup>[36]</sup> In the constant heat-flux theory, the  $\Delta T$  in a closed circuit ( $\Delta T_{cc}$ ) and the  $\eta_{TE}$  as a function of  $s$  at conditions of  $C_r = 40$ ,  $T_{c,oc} = 285.4 \text{ K}$  (the temperature on the cold side in an open circuit, is generally assumed unchanged in theoretical analysis),  $\xi_{ab} = 0.1$ , and  $E_g = 1.4 \text{ eV}$ , are presented in **Figure 5**. In an open circuit, only Fourier heat exists across TEG and the  $\Delta T$  across TEG ( $\Delta T_{oc}$ ) remains unchanged. Clearly, the Peltier heat and Joule heat strengthen as  $ZT$  increases in a closed circuit, and the  $\Delta T$  across TEG decreases. For a given  $ZT$ , the  $\Delta T$  across TEG

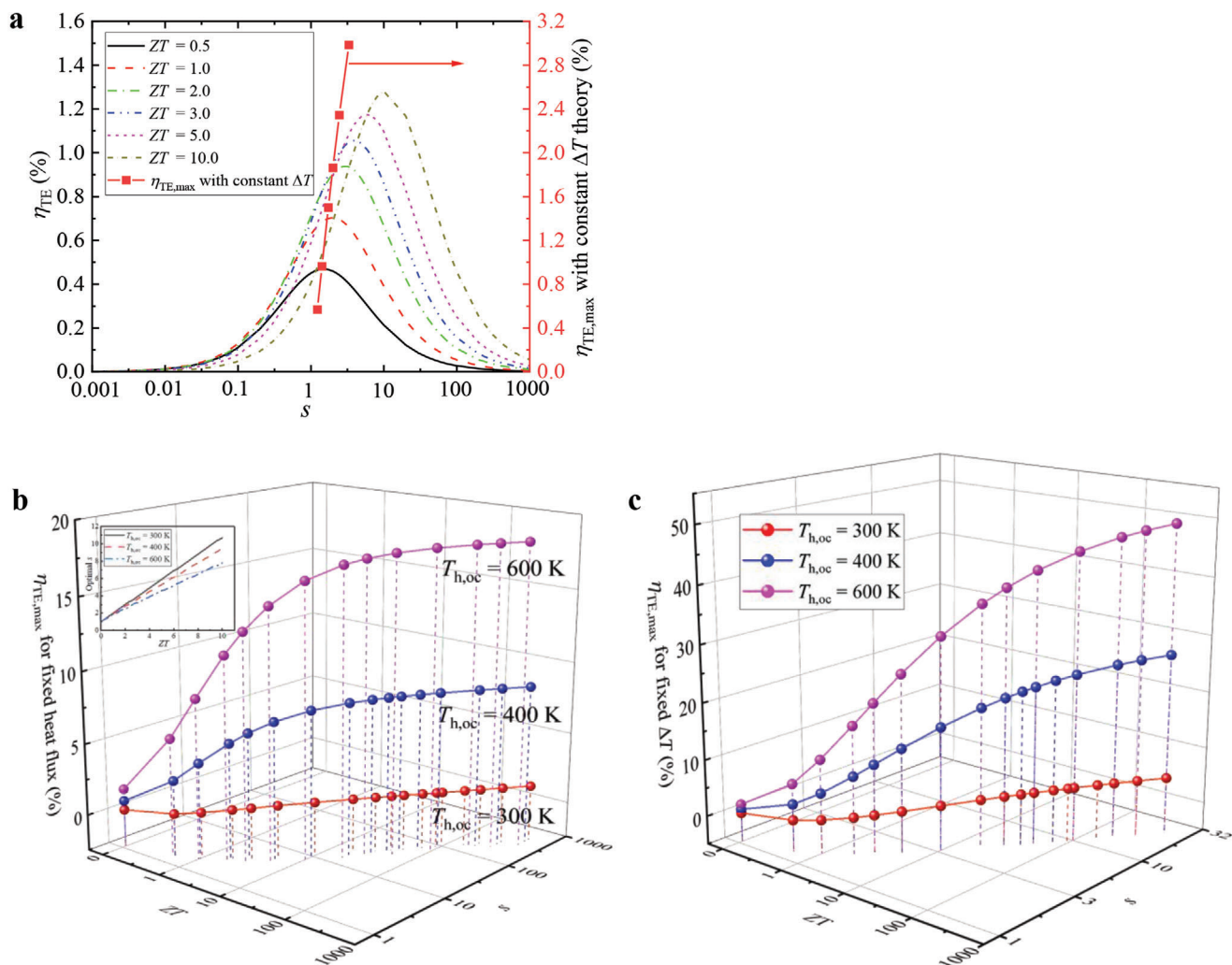


**Figure 6.** TE efficiencies obtained with constant heat-flux and temperature-difference theories. a) TE efficiencies obtained with the two theories at night,  $T_{h,oc} = 300$  K. b) Maximum TE efficiency obtained with constant heat-flux theory. c) Maximum TE efficiency obtained with constant  $\Delta T$  theory. Other condition:  $T_{c,oc} = 283.53$  K.

increases as the ratio  $s$  increases. In the case of  $s = 0$ , TEG is in a short circuit, the current is the maximum, and the  $\Delta T$  across TEG is the smallest, and also decreases as  $ZT$  increases due to the stronger Peltier heat and Joule heat. In the case of  $s = \infty$ , TEG is in an open circuit, the  $\Delta T$  across TEG is  $\Delta T_{oc}$ .

In constant heat-flux theory, the  $\eta_{TE}$  increases first as the ratio  $s$  increases, reaches a peak and then decreases as shown in Figure 5b. The peak value of  $\eta_{TE}$  increases as  $ZT$  increases, from 4.7% at  $ZT = 0.5$  to 13.3% at  $ZT = 10$ . The optimal ratio  $s_{opt}$  that corresponds to the peak of  $\eta_{TE}$  for a given  $ZT$ , also increases as  $ZT$  rises, from 1.5 at  $ZT = 0.5$  to 8 at  $ZT = 10$ . At  $ZT = 1.0$ , the  $s_{opt}$  is 1.9, that is different from the constant  $\Delta T$  theory in which the maximal output power corresponds to  $s_{opt} = 1$  and the maximal  $\eta_{TE}$  corresponds to Equation (10). Figure 5a,b shows that decreasing  $s$  leads to reducing  $\Delta T$  across TEG, resulting in the reduction of voltage difference across TEG, while the decreasing  $s$  results in an increase of current. Therefore, there exists an  $s_{opt}$  in which current and voltage reach trade-off, leading to a peak of  $\eta_{TE}$ . At  $E_g = 1.4$  eV and  $Z = 2 \times 10^{-3} \text{ K}^{-1}$ , the peak value of  $\eta_{TE}$  in-

creases significantly as  $C_r$  increases as shown in Figure 5c, from 1.8% at  $C_r = 10$  to 7.6% at  $C_r = 50$ . While the  $s_{opt}$  corresponding to the maximum  $\eta_{TE}$  slightly increases as  $C_r$  increases with constant heat-flux theory, from 1.6 at  $C_r = 10$  to 1.7 at  $C_r = 50$ . At conditions of  $C_r = 40$ ,  $Z = 2 \times 10^{-3} \text{ K}^{-1}$ , and  $T_{c,oc} = 285.4$  K, the peak value of  $\eta_{TE}$  increases largely as the material's  $E_g$  increases, from 0.9% at  $E_g = 0.66$  eV to 9.5% at  $E_g = 1.81$  eV, while the  $s_{opt}$  slightly increases from 1.6 at  $E_g = 0.66$  eV to 1.8 at  $E_g = 1.81$  eV. This indicates that the  $s_{opt}$  is mainly influenced by  $ZT$  while heat flux also affects the  $s_{opt}$  in constant heat-flux theory.

For a given  $\Delta T_{oc}$ , the  $\eta_{TE}$  obtained with constant heat-flux and temperature-difference theories are presented in Figure 6. At night, the temperature on the cold side reaches 283.53 K via the radiative cooler, while the temperature on the hot side keeps the same as the ambient temperature ( $T_a = 300$  K). In this case, the ambient is employed as the heat source whose heat capacity is very large, and the TEG is viewed as operating under a constant temperature-difference condition ( $T_{h,oc} = 300$  K and  $T_{c,oc} = 283.53$  K), and its efficiency is shown in Figure 6a.



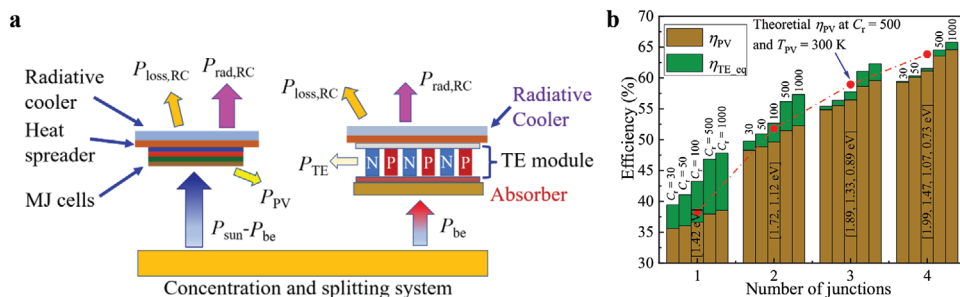


**Figure 7.** SS MJ PV-TE-RC system and its efficiency. a) A concentrated SS MJ PV-TE-RC system. b) Efficiencies in these systems with various  $C_r$ , at conditions of  $R_c = C_r$ ,  $ZT = 2$ , and  $\xi_{\text{ab}} = 0.1$ .

The peak value of  $\eta_{\text{TE}}$  obtained with constant heat-flux theory increases as  $ZT$  rises, from 0.5% at  $ZT = 0.5$  to 1.3% at  $ZT = 10$ , and the corresponding  $s_{\text{opt}}$  increases from 1.5 at  $ZT = 1.5$  to 10.7 at  $ZT = 10$ . The  $\eta_{\text{TE,max}}$  obtained with constant  $\Delta T$  theory increases greatly from 0.6% at  $ZT = 0.5$  to 3% at  $ZT = 10$ , and the corresponding  $s_{\text{opt}}$  increases from 1.2 at  $ZT = 0.5$  to 3.3 at  $ZT = 10$  following Equation (10). It is clear that the  $\eta_{\text{TE,max}}$  obtained with constant  $\Delta T$  theory is higher than that obtained with the constant heat-flux theory, and the absolute difference between the two  $\eta_{\text{TE,max}}$  increases as  $ZT$  increases, from 0.1% at  $ZT = 0.5$  to 1.7% at  $ZT = 10$ .

The temperature on the cold side remains unchanged at  $T_{\text{c,oc}} = 283.53$  K, the temperature on the hot side increases to 400 and 600 K (i.e.,  $T_{\text{h,oc}} = 400$  K and  $T_{\text{h,oc}} = 600$  K), the  $\eta_{\text{TE,max}}$  obtained with the constant heat-flux and  $\Delta T$  theories as a function of  $ZT$  and  $s$  are presented in Figure 6b,c. In the constant heat-flux theory, the  $s_{\text{opt}}$  increases as  $ZT$  increases for a given  $T_{\text{h,oc}}$ , and also slightly increases as  $T_{\text{h,oc}}$  increases for a given  $ZT$ . For example, the  $s_{\text{opt}}$  increases from 1.9 at  $ZT = 1$  to 9.5 at  $ZT = 10$  with  $T_{\text{h,oc}} = 400$  K, and decreases slightly from 2 at  $T_{\text{h,oc}} = 300$  K to 1.8 at  $T_{\text{h,oc}} = 600$  K with  $ZT = 1$ . In constant  $\Delta T$  theory, the  $s_{\text{opt}}$  slightly increases with  $ZT$ , and is not affected by  $T_{\text{h,oc}}$ . In constant heat-flux theory, the  $\eta_{\text{TE,max}}$  increases significantly as  $ZT$  increases in the case of  $ZT < 10$ , while it increases very slightly in the case of  $ZT > 10$ , so it is more cost-effective to make  $ZT < 10$  in actual design of TEG. In the case of  $ZT < 10$ , the  $s_{\text{opt}}$  increases approximately linearly with  $ZT$  in constant heat-flux theory as shown in Figure 6b, and the fitting formulas between them are as follows

$$\begin{aligned} s_{\text{opt}} &= 0.97 \cdot ZT + 1.02, \text{ at } T_{\text{h,oc}} = 300 \text{ K} \\ s_{\text{opt}} &= 0.84 \cdot ZT + 1.09, \text{ at } T_{\text{h,oc}} = 400 \text{ K} \\ s_{\text{opt}} &= 0.67 \cdot ZT + 1.18, \text{ at } T_{\text{h,oc}} = 600 \text{ K} \end{aligned} \quad (12)$$

#### 2.4. Spectral-Splitting MJ PV-TE System

To get as much electricity as possible from the sun, MJ cells are employed to reduce the thermalization heat, namely, the single-junction PV cell in Figure 3 is replaced by MJ cells (as shown in Figure 7a). The  $E_g$  of MJ cells given in ref. [37] is adopted in this section, which is listed in Figure 7b. In this SS MJ PV-TE system, the solar spectrum with photon energy below the minimum  $E_g$  is directed to the absorber to be utilized by TEG. The photons with energy above the minimum  $E_g$  are utilized by the cell with

matching  $E_g$ , and the thermalization heat is dissipated through the radiative cooler placed above the PV panel.

Five concentration ratios ( $C_r = 30, 50, 100, 500$ , and 1000) are selected to investigate the efficiency of the SS MJ cells system, where  $C_r = 100$  is taken as a typical concentration ratio in a current parabolic trough or parabolic dish,  $C_r = 1000$  is taken as a typical concentration ratio of current solar towers,<sup>[38]</sup> and  $C_r = 500$  is taken as typical moderate concentration ratio. Although  $C_r = 46000$  is generally taken as the maximum concentration ratio achievable on earth,<sup>[39]</sup>  $C_r = 1000$  is taken as the maximum concentration ratio in this study, considering the temperature that materials can withstand, the uniformity of temperature in heat spreader of radiative cooler, cost, covered area, etc. The  $\eta_{\text{TE,eq}}$  decreases as the number of junctions increases, while increases as  $C_r$  increases. For example, at  $C_r = 50$ ,  $\eta_{\text{TE,eq}}$  is 5% for one junction, 2.1% for two junctions, 0.8% for three junctions, and 0.2% for four junctions. In the system with two-junction cells,  $\eta_{\text{TE,eq}}$  increases from 1.5% at  $C_r = 30$  to 5.1% at  $C_r = 1000$ . In the system with four-junction cells,  $\eta_{\text{TE,eq}}$  is about 1.2% at  $C_r = 1000$ , so it is less significant to discuss the MJ PV-TE system when the number of junctions is higher than 4.  $\eta_{\text{PV}}$  and  $\eta_{\text{TE,eq}}$  increase as  $C_r$  and the number of junctions increase, while the increasing margin recedes as the number of junctions increases. The theoretical efficiency of PV panel at  $C_r = 500$  and  $T_{\text{PV}} = 300$  K is employed as a reference efficiency. In the single-junction cell system,  $\eta_{\text{PV+TE}}$  at  $C_r = 30$  is 39.4% that is higher than the theoretical  $\eta_{\text{PV}}$  at  $C_r = 500$  and  $T_{\text{PV}} = 300$  K (38.2%); and  $\eta_{\text{PV+TE}}$  at  $C_r = 500$  is 55.6% that is an absolute increment of more than 17 percentage points relative to the reference efficiency. In the two-junction cells,  $\eta_{\text{PV+TE}}$  at  $C_r = 100$  is 52.7% that is higher than the theoretical  $\eta_{\text{PV}}$  at  $C_r = 500$  and  $T_{\text{PV}} = 300$  K (51.8%), and  $\eta_{\text{PV+TE}}$  at  $C_r = 500$  is 56.2% that is an absolute increment of more than 4.4 percentage points relative to the reference efficiency. In the three-junction cells,  $\eta_{\text{PV+TE}}$  at  $C_r = 500$  is 61.1% which is an absolute increment of more than 2.2 percentage points relative to the reference efficiency (58.9%). In the four-junction cells,  $\eta_{\text{PV+TE}}$  at  $C_r = 500$  is 64.5% which is an absolute increment of more than 0.7 percentage points relative to the reference efficiency (63.8%). This indicates that the SS MJ PV-TE-RC system is more suitable for the system with a small number of junctions ( $\leq 3$ ), this is in line with the actual situation, that is the greater number of junctions leads to soaring cost and manufacturing difficulty. At  $C_r = 1000$ ,  $\eta_{\text{PV+TE}}$  increases from 48% to 66% as the number of junctions rises from 1 to 4, and the  $\eta_{\text{PV+TE}}$  in the hybrid system

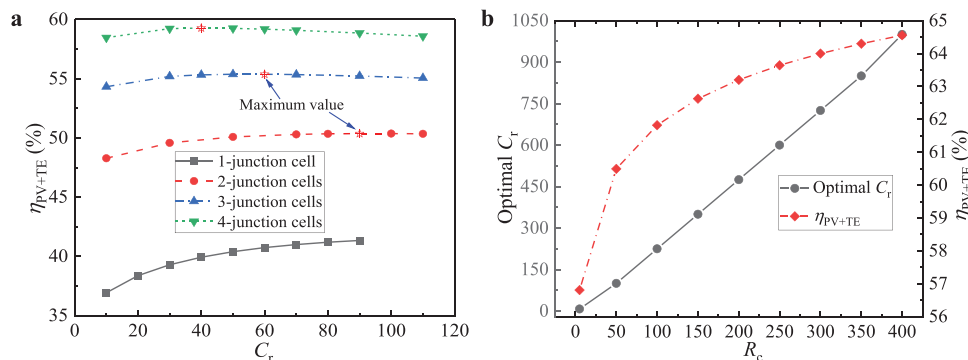


**Figure 8.**  $\eta_{PV+TE}$  in SS MJ PV-TE-RC systems. a)  $\eta_{PV+TE}$  in the systems as a function of  $C_r$  at  $R_c = 25$ . b) The optimal  $C_r$  that maximizes  $\eta_{PV+TE}$  and its corresponding  $\eta_{PV+TE}$  as a function of  $R_c$  in the system including four-junction cells. Other conditions:  $ZT = 2$  and  $\xi_{ab} = 0.1$ .

including four-junction cells is over 65%, which outperforms most current photoelectric and thermal power systems.

The  $\eta_{PV+TE}$  as a function of  $C_r$  and  $R_c$  is demonstrated in Figure 8. At  $R_c = 25$  and  $\xi_{ab} = 0.1$ , as  $C_r$  increases from 10 to 90,  $\eta_{PV+TE}$  in the system with one-junction cell monotonously increases from 36.9% to 41.2% as shown in Figure 8a, while  $\eta_{PV+TE}$  in the systems with MJ cells increases first and then decreases.  $\eta_{PV+TE}$  in the system with two-junction cells reaches a peak of 50.4% at  $C_r = 90$ ,  $\eta_{PV+TE}$  in the system with three-junction cells reaches a peak of 55.4% at  $C_r = 60$ ,  $\eta_{PV+TE}$  in the system with four-junction cells reaches a peak of 59.3% at  $C_r = 40$ . A larger number of junctions in the system means a smaller optimal  $C_r$  that corresponds to the maximum  $\eta_{PV+TE}$  for a given  $R_c$ . Since the proportion of  $\eta_{PV}$  in the  $\eta_{PV+TE}$  rises as the number of junctions increases, the changing trend of  $\eta_{PV+TE}$  is more dependent on  $\eta_{PV}$ . In the four-junction hybrid system, the optimal  $C_r$  at which  $\eta_{PV+TE}$  reaches the maximum and its corresponding  $\eta_{PV+TE}$  as a function of  $R_c$  are demonstrated in Figure 8b. The optimal  $C_r$  increases nearly linearly as  $R_c$  rises, the ratio of the optimal  $C_r$  to  $R_c$  increases slightly as  $R_c$  increases and the average ratio is 2.3 in the range of parameters selected in this study.  $\eta_{PV+TE}$  increases as  $R_c$  rises while the increasing slope declines. Of note is that the  $\eta_{PV+TE}$  when optimal  $C_r$  is 1000 is less than  $\eta_{PV+TE}$  at  $C_r = 1000$  in Figure 7b, since  $R_c$  is much higher in the latter ( $R_c = 1000$ ) than in the former ( $R_c = 400$ ). This indicates that  $R_c$  can be far less than  $C_r$  in practice, but increasing  $R_c$  is one of the most effective ways to improve efficiency.

### 3. Discussion and Conclusions

The bandgap energy ( $E_g$ ) generally decreases with increasing  $T_{PV}$ , especially at high temperature of  $T_{PV} > 200$  °C, which will affect  $\eta_{PV}$ . If the temperature difference between the ambient and PV cell is not beyond 100 °C, the  $\eta_{PV}$  extrapolated based on the  $E_g$  at  $T_a$  is very accurate (almost exactly identical with the  $\eta_{PV}$  using  $E_g$  as a function of  $T_{PV}$ ) for most PV materials as demonstrated in ref. [40]. The  $T_{PV}$  is limited to no more than 373 K and  $T_a$  is fixed at 300 K in this study, so it is reasonable to assume that  $E_g$  remains its value at  $T_a$  without variation with  $T_{PV}$  in this study for the convenience of calculation, and the results are accurate and reliable.

The PV material's  $E_g$  has an important influence on  $\eta_{PV+TE}$  as shown in Figure 4a, the  $E_g$  in the systems with MJ cells in Fig-

ure 7 is from ref. [37] without considering the addition of TEG. Therefore,  $\eta_{PV+TE}$  in SS MJ PV-TE-RC system can be further improved by optimizing the combination of  $E_g$  in MJ cells, considering the properties of PV cells and TEG. Heat flux and temperature difference affect each other in practice, there is no definite constant temperature-difference or heat-flux condition, just which changes faster. As far as the characteristics of solar energy itself are concerned, it is more reasonable to regard it as a constant heat-flux condition.

The  $\Delta T$  across TEG in a closed circuit will be lower than that in an open circuit due to the Peltier heat, and the maximum gap occurs when the ratio  $s$  is 0 (in a short circuit). There exists an optimal  $s$  in which  $\eta_{TE}$  reaches the maximum for a given  $ZT$ , the optimal  $s$  increases almost linearly as  $ZT$  increases, and also increases slightly as  $C_r$  and PV material's  $E_g$  increase.

In the PV-TE-RC system with a single-junction cell in Figure 1d, a temperature lower than  $T_a$  is achieved via a radiative cooler, so the  $\eta_{PV+TE}$  (33.8%) is higher than that in the conventional PV-TE system in Figure 1c (33.1%). Moreover, a  $\eta_{TE,eq}$  of 0.4% can be achieved at night. At  $R_c = 20$ , the  $\eta_{tot}$  increases and then decreases as  $C_r$  rises, reaches a peak (34.3%) at  $C_r = 3$ , since the increasing  $T_{PV}$  is inductive to TEG but deteriorates  $\eta_{PV}$ . The increasing  $R_c$  is beneficial to PV panel and TEG at the same time.

SS PV-TE-RC system with a single-junction cell is more suitable for a high  $C_r$ , and the PV material's  $E_g$  has a crucial influence on the TEG. Generally,  $\eta_{TE}$  increases as  $E_g$  and  $C_r$  increase, while the system with PV material GaAs ( $E_g = 1.42$  eV) has the highest  $\eta_{tot}$  among the four PV materials (Ge, Si, GaAs, GaInP). For a given  $R_c$ , there exists an optimal  $C_r$  at which  $\eta_{PV}$  reaches the maximum, while the optimal  $C_r$  that maximizes  $\eta_{PV+TE}$  depends on the ratio of  $\eta_{TE}$  to  $\eta_{PV}$ , and a smaller ratio indicates a smaller optimal  $C_r$ .

In the SS PV-TE-RC system with MJ cells, there exists an optimal  $C_r$  at which  $\eta_{PV+TE}$  reaches the maximum for a given  $R_c$  when the number of junctions is not less than 2. The optimal  $C_r$  decreases as the number of junctions increases, and the ratio of optimal  $C_r$  to  $R_c$  increases slightly as  $R_c$  grows. Generally,  $\eta_{PV}$  and  $\eta_{PV+TE}$  increase as the number of junctions increases while  $\eta_{TE}$  decreases quickly. At  $C_r = 100$ ,  $\eta_{PV+TE}$  in the system with two-junction cells (52.7%) is higher than the corresponding theoretical  $\eta_{PV}$  at  $C_r = 500$  and  $T_{PV} = 300$  K (51.8%). At  $C_r = 500$ ,  $\eta_{PV+TE}$  in the system with three-junction and four-junction cells (61.1% and 64.5%) are higher than the corresponding theoretical  $\eta_{PV}$  at

$T_{PV} = 300$  K (58.9% and 63.8%), while the gap decreases as the number of junctions increases.  $\eta_{PV+TE}$  in a single-junction cell system at  $C_r = 30$  (39.4%) is higher than the theoretical  $\eta_{PV}$  at  $C_r = 500$  and  $T_{PV} = 300$  K (38.2%), demonstrating the huge advantages of the SS PV-TE-RC system, especially when the number of junctions is small.  $\eta_{PV+TE}$  is over 65% at  $C_r = 1000$  in the system with four-junction cells which is superior to most current photovoltaic and thermal power systems.

#### 4. Experimental Section

**Hybrid PV-TE Model:** The present model is based on the following assumptions: 1) the quantum efficiency of the solar cells is 1 and the solar cells are ideal; 2) the losses of optical devices including concentrator and SS filter are negligible; 3) the diurnal ambient temperature ( $T_a$ ) is fixed at 300 K, and the sunlight is AM1.5 spectral irradiation (as shown in Figure 1a); 4) each photon whose energy exceeds  $E_g$  excites one electron-hole pair, and the excess energy above  $E_g$  dissipates as waste heat in solar cells; 5) the thermal resistances between solar cells and TE module, and between TE module and RC are negligible; 6) the transverse heat loss between the TE module and the ambient is negligible; 7) the solar cells remain the same temperature with the ambient at night.

The photons emitted by a blackbody with temperature  $T$  according to Planck's law read<sup>[41]</sup>

$$\phi_{bb}(E, T) = \frac{2\pi}{h^3 c^2} \frac{E^2}{\exp[E/(k_b T)] - 1} \quad (13)$$

where  $h$  is the Planck's constant,  $k_b$  is the Boltzmann constant,  $c$  is the speed of light, and the subscript "bb" represents blackbody. The spectral energy flux of the black body had the expression

$$I_{bb}(E, T) = E\phi_{bb}(E, T) \quad (14)$$

where  $E$  is the photon energy. According to the above assumptions, the thermalization heat of a PV cell read<sup>[42]</sup>

$$P_{th} = \int_{E_g}^{\infty} C_r A_{PV} (E - E_g) \phi_{AM1.5} dE \quad (15)$$

The spectral energy below  $E_g$  that cannot be utilized by PV cell could be written as<sup>[42]</sup>

$$P_{be} = \int_0^{E_g} C_r A_{PV} E \phi_{AM1.5} dE \quad (16)$$

Thus, the thermal balance of a PV cell could be written as

$$P_{th} + P_{be} = \epsilon_{PV} \sigma (2A_{PV} - N_{TE} A_{TE}) (T_{PV}^4 - T_a^4) + h_c (2A_{PV} - N_{TE} A_{TE}) (T_{PV} - T_a) + Q_{TE} \quad (17)$$

where  $\epsilon$  is the emissivity,  $\sigma$  is the Stefan-Boltzmann constant,  $Q_{TE}$  is the heat transferred from PV cell to TE module. The heat transfer coefficient  $h_c$  is mainly affected by wind speed, the relevant expressions of  $h_c$  as a function of wind speed are summarized in refs. [1b, 43]. It is generally recommended  $h_c = 5 \text{ W m}^{-2} \text{ K}^{-1}$  in light breeze and  $h_c = 40 \text{ W m}^{-2} \text{ K}^{-1}$  at strong breeze,  $h_c$  could be reduced by windshield or vacuum in practice. The default  $h_c$  was  $5 \text{ W m}^{-2} \text{ K}^{-1}$  for the convenience of calculation in this study, unless otherwise specified. The heat transferred from PV cell to TE module read<sup>[44]</sup>

$$Q_{TE} = \frac{k_{TE} N_{TE} A_{TE} [1 + Z(3T_{PV} + T_c)/8] (T_{PV} - T_c)}{L_{TE}} \quad (18)$$

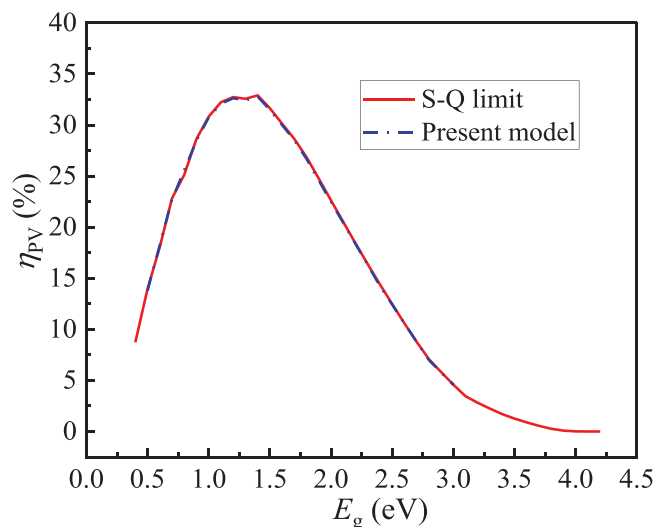


**Figure 9.** The  $\eta_{PV}$  in the present model and the S-Q limit as a function of  $E_g$ .

where  $k_{TE}$  is the thermal conductivity of TE material ( $k_{TE} = 1.5 \text{ W m}^{-1} \text{ K}^{-1}$ ).

The current of a single-junction solar cell under solar irradiance could be written as<sup>[45]</sup>

$$J_{PV} = J_L - J_0 \left[ \exp\left(\frac{qV_{PV}}{nk_b T_{PV}}\right) - 1 \right] \quad (19)$$

where  $J_L$  is the photogenerated current,  $J_0$  is the reverse saturation current,  $n$  is the ideal factor with  $n = 1$  for ideal p-n junctions,  $q$  is the elementary charge,  $V$  is the voltage. The open-circuit (oc) voltage could be deduced from Equation (19) with  $J_{PV} = 0$

$$V_{oc} = \frac{nk_b T_{PV}}{q} \ln\left(\frac{J_L}{J_0} + 1\right) \quad (20)$$

The ideal PV power could be written as

$$P_{PV} = V_{oc} \cdot J_{sc} \cdot FF \quad (21)$$

where  $J_{sc}$  is the short circuit current of PV cell and  $FF$  is the fill factor. The PV efficiency obtained in the present model had a good agreement with the well-known S-Q limit as shown in **Figure 9**, validating the reliability of the present model.

**Thermoelectric Efficiency under Constant Heat-Flux Conditions:** For a TE module working at temperature difference  $\Delta T$ , the electrical current read

$$I = \frac{\alpha \cdot \Delta T}{R_L + R_i} \quad (22)$$

The voltage across the module read

$$V = \frac{N_{TE} \alpha \cdot \Delta T \cdot s}{1 + s} \quad (23)$$

The thermoelectrical conversion efficiency could be written as

$$\eta_{TE, \Delta T} = \frac{\left(1 - \frac{T_c}{T_h}\right) s}{(1 + s) - \frac{1}{2} \left(1 - \frac{T_c}{T_h}\right) + \frac{1}{2ZT} (1 + s)^2 \left(1 + \frac{T_c}{T_h}\right)} \quad (24)$$

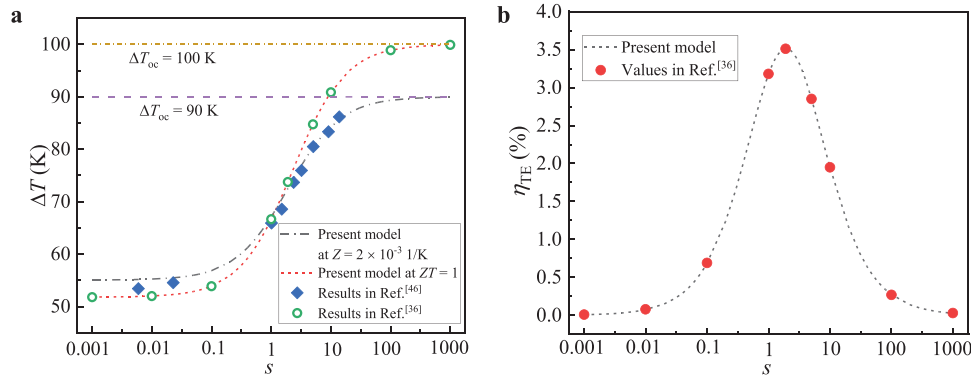


**Figure 10.** Comparison between the results obtained in the present model and in literatures. a) The temperature differences under a closed-circuit state obtained in this study against the results at  $\Delta T_{oc} = 90$  K in ref. [46] and at  $\Delta T_{oc} = 100$  K in ref. [36]. b) TE efficiency obtained in the present work against the results at  $\Delta T_{oc} = 100$  K in ref. [36].

The maximum conversion efficiency could be obtained by differentiating Equation (24) with respect to the ratio  $s$  and setting it to zero, yielding Equations (9) and (10) above.

However, Equation (9) would become invalid under constant heat-flux condition, to address this issue, a new theory was established for TEG operating under constant heat-flux condition recently.<sup>[36]</sup> The key to the new theory was the relationship between the  $\Delta T$  across TEG under open-circuit and closed-circuit conditions, which was written as<sup>[36,44]</sup>

$$\Delta T_{oc} = \Delta T_{cc} (1 + ZT_m) \quad (25)$$

with

$$T_m = \frac{(1 + 2s)T_{h,cc} + T_{c,cc}}{2(1 + s)^2} \quad (26)$$

where subscript “oc” and “cc” denote open circuit and closed circuit, and subscript “h” and “c” denote hot and cold. Therefore, the voltage and current under heat-flux condition in a closed circuit could be written as

$$V_{cc} = \frac{\alpha \Delta T_{oc}}{1 + ZT_m} \frac{R_L}{R_i + R_L} \quad (27)$$

$$I_{cc} = \frac{\alpha \Delta T_{oc} / (1 + ZT_m)}{R_i + R_L} \quad (28)$$

Finally, the TE power and TE efficiency could be written as follows<sup>[36]</sup>

$$P_{TE} = \frac{(\alpha \Delta T_{oc})^2 s}{R_i (1 + ZT_m)^2 (1 + s)^2} \quad (29)$$

$$\eta_{TE} = \frac{Z \Delta T_{oc} s}{(1 + ZT_m)^2 (1 + s)^2} \quad (30)$$

The temperature difference and efficiency of TEG obtained in this study against the results in literature are presented in **Figure 10**. At  $\Delta T_{oc} = 100$  K, the temperature difference and efficiency obtained in this study had good agreement with the results in ref. [36]. At  $\Delta T_{oc} = 90$  K, the temperature difference obtained in this study was in good agreement with the results given in ref. [46] between  $s = 1$  and  $s = 10$ , although the results obtained in this study were slightly higher in the range of  $s < 0.1$ . Of note was that the results discussed in this study were mainly concentrated between  $s = 1$  and  $s = 10$ , therefore, the calculation results about TEG were reliable and acceptable in this study.

**Radiative Cooling:** The thermal energy emitted by a material with an emissivity of  $\epsilon_{RC}(\lambda, \theta)$  could be written as

$$\begin{aligned} P_{rad,RC}(T_{RC}) &= \int_{\Omega} \cos \theta \int_0^{\infty} R_c A_{PV} \epsilon_{RC}(\lambda, \theta) I_{bb}(\lambda, T_{RC}) d\lambda d\Omega \\ &= 2\pi \int_0^{\pi/2} \int_0^{\infty} R_c A_{PV} \epsilon_{RC}(\lambda, \theta) I_{bb}(\lambda, T_{RC}) \sin \theta \cos \theta d\lambda d\theta \end{aligned} \quad (31)$$

where  $\theta$  denotes the angle between the direction of the solid angle and the normal direction of the surface,  $\Omega$  is the solid angle.

The solar power that was absorbed by the radiative cooler read

$$P_{sun,RC} = \int_0^{\infty} I_{AM1.5}(\lambda) R_c A_{PV} \epsilon_{RC}(\lambda, \theta_{sun} = 0) d\lambda \quad (32)$$

where  $\theta_{sun}$  denotes the direction of incident sunlight. The  $\theta_{sun}$  was assumed to be 0 so as to maximize solar spectral irradiance.

The power absorbed by RC from the atmosphere via radiation could be written as

$$\begin{aligned} P_{atm,RC}(T_a) &= 2\pi \int_0^{\pi/2} \int_0^{\infty} I_{bb}(\lambda, T_a) R_c A_{PV} \epsilon_{atm}(\lambda, \theta) \epsilon_{RC}(\lambda, \theta) \\ &\quad \sin \theta \cos \theta d\lambda d\theta \end{aligned} \quad (33)$$

where  $\epsilon_{atm}$  is the atmospheric emissivity, which was given by<sup>[47]</sup>

$$\epsilon_{atm}(\lambda, \theta) = 1 - \tau_{atm}(\lambda)^{\cos \theta} \quad (34)$$

where  $\tau_{atm}$  is the atmospheric transmittance in the zenith direction.

Lastly, the cooling power of the radiative cooler was written as

$$\begin{aligned} P_{cool}(T_{RC}) &= P_{rad,RC}(T_{RC}) - P_{sun,RC} - P_{atm,RC}(T_a) - Q_{in} \\ &\quad - h_c R_c A_{PV} (T_a - T_{RC}) \end{aligned} \quad (35)$$

where  $Q_{in}$  represents the heat entering the radiative cooler from PV panel or TEG, and the last term on the right of Equation (35) denotes the heat entering from the ambient.

## Acknowledgements

This project has received funding from the CAS Project for Young Scientists in Basic Research (grant no. YSBR-043). The research was also

supported by the European Union's Horizon 2020 research and innovation programme under the Marie Skłodowska-Curie grant agreement no. [882628]. For the purpose of Open Access, the authors have applied a CC BY public copyright license to any Author Accepted Manuscript version arising from this submission.

## Conflict of Interest

The authors declare no conflict of interest.

## Data Availability Statement

The data that support the findings of this study are available from the corresponding author upon reasonable request.

## Keywords

concentrated spectral splitting, multi-junction cells, photovoltaic, radiative cooling, solar energy, thermoelectric generator

Received: November 9, 2022

Revised: January 6, 2023

Published online: February 7, 2023

- [1] a) M. Sharaf, M. S. Yousef, A. S. Huzayyin, *Environ. Sci. Pollut. Res.* **2022**, 29, 26131; b) R. Vilà, I. Martorell, M. Medrano, A. Castell, *Sol. Energy Mater. Sol. Cells* **2021**, 230, 111275.
- [2] a) T. J. Jacobsson, A. Hultqvist, A. García-Fernández, A. Anand, A. Al-Ashouri, A. Hagfeldt, A. Crovetto, A. Abate, A. G. Ricciardulli, A. Vijayan, A. Kulkarni, A. Y. Anderson, B. P. Darwich, B. Yang, B. L. Coles, C. A. R. Perini, C. Rehermann, D. Ramirez, D. Fairen-Jimenez, D. Di Girolamo, D. Jia, E. Avila, E. J. Juarez-Perez, F. Baumann, F. Mathies, G. S. A. González, G. Boschloo, G. Nasti, G. Paramasivam, G. Martínez-Denegri, *Nat. Energy* **2022**, 7, 107; b) I. Massiot, A. Cattoni, S. Collin, *Nat. Energy* **2020**, 5, 959; c) E. Rahman, A. Nojeh, *Nat. Commun.* **2021**, 12, 4622.
- [3] W. Shockley, H. J. Queisser, *J. Appl. Phys.* **1961**, 32, 510.
- [4] P. T. Landsberg, G. Tonge, *J. Appl. Phys.* **1980**, 51, R1.
- [5] a) E. Skoplaki, J. A. Palyvos, *Sol. Energy* **2009**, 83, 614; b) J. Dumoulin, E. Drouard, M. Amara, *Sustainable Energy Fuels* **2021**, 5, 2085.
- [6] a) J. Wu, X. Zhang, J. Shen, Y. Wu, K. Connelly, T. Yang, L. Tang, M. Xiao, Y. Wei, K. Jiang, C. Chen, P. Xu, H. Wang, *Renewable Sustainable Energy Rev.* **2017**, 75, 839; b) G. Huang, K. Wang, C. N. Markides, *Light: Sci. Appl.* **2021**, 10, 28; c) R. R. King, D. Bhusari, A. Boca, D. Larrabee, X. Q. Liu, W. Hong, C. M. Fetzer, D. C. Law, N. H. Karam, *Prog. Photovoltaics* **2011**, 19, 797; d) Y. Park, B. Zhao, S. Fan, *Nano Lett.* **2022**, 22, 448.
- [7] M. I. Hossain, *J. Phys. D: Appl. Phys.* **2014**, 47, 075101.
- [8] a) T. M. Tritt, H. Böttner, L. Chen, *MRS Bull.* **2008**, 33, 366; b) X. Ju, Z. Wang, G. Flamant, P. Li, W. Zhao, *Sol. Energy* **2012**, 86, 1941.
- [9] E. Elsarrag, H. Pernau, J. Heuer, N. Roshan, Y. Alhorr, K. Bartholomé, *Renewables: Wind, Water, Sol.* **2015**, 2, 16.
- [10] E. Yin, Q. Li, Y. Xuan, *Energy* **2018**, 163, 519.
- [11] M. Alnajideen, G. Min, *Energy Convers. Manage.* **2022**, 251, 114981.
- [12] M. A. I. Khan, M. I. Khan, A. H. Kazim, A. Shabir, F. Riaz, N. Mustafa, H. Javed, A. Raza, M. Hussain, C. A. Salman, *Front. Energy Res.* **2021**, 9, 722514.
- [13] a) D. Kraemer, B. Poudel, H.-P. Feng, J. C. Caylor, B. Yu, X. Yan, Y. Ma, X. Wang, D. Wang, A. Muto, K. McEnaney, M. Chiesa, Z. Ren, G. Chen, *Nat. Mater.* **2011**, 10, 532; b) D. Kraemer, Q. Jie, K. McEnaney, F. Cao, W. Liu, L. A. Weinstein, J. Loomis, Z. Ren, G. Chen, *Nat. Energy* **2016**, 1, 16153.
- [14] H. T. Hashim, Ph.D. Thesis, Cardiff University, XX **2015**.
- [15] C. Lertsatitthanakorn, J. Jamradloedluk, M. Rungsitopas, *J. Electron. Mater.* **2013**, 42, 2119.
- [16] A. Liu, H. Xie, Z. Wu, Y. Wang, *Carbon Neutrality* **2022**, 1, 20.
- [17] a) S. Fan, W. Li, *Nat. Photonics* **2022**, 16, 182; b) X. Yin, R. Yang, G. Tan, S. Fan, *Science* **2020**, 370, 786; c) J. Mandal, Y. Fu, C. Overvig Adam, M. Jia, K. Sun, N. Shi Norman, H. Zhou, X. Xiao, N. Yu, Y. Yang, *Science* **2018**, 362, 315; d) G. Smith, A. Gentle, *Nat. Energy* **2017**, 2, 17142.
- [18] A. P. Raman, M. A. Anoma, L. Zhu, E. Rephaeli, S. Fan, *Nature* **2014**, 515, 540.
- [19] Z. Chen, L. Zhu, A. Raman, S. Fan, *Nat. Commun.* **2016**, 7, 13729.
- [20] L. Zhu, A. Raman, K. X. Wang, M. A. Anoma, S. Fan, *Optica* **2014**, 1, 32.
- [21] M. Gao, Y. Xia, R. Li, Z. Zhang, Y. He, C. Zhang, L. Chen, L. Qi, Y. Si, Q. Zhang, Y. Zheng, *Nanomaterials* **2020**, 10, 2483.
- [22] Z. Wang, D. Kortge, J. Zhu, Z. Zhou, H. Torsina, C. Lee, P. Bermel, *Joule* **2020**, 4, 2702.
- [23] Z. Li, S. Ahmed, T. Ma, *Sol. RRL* **2021**, 5, 2000735.
- [24] W. Li, Y. Shi, K. Chen, L. Zhu, S. Fan, *ACS Photonics* **2017**, 4, 774.
- [25] a) G. Ulpiani, G. Ranzi, J. Feng, M. Santamouris, *Energy Build.* **2021**, 243, 110990; b) S. Ahmed, Z. Li, M. S. Javed, T. Ma, *Mater. Today Energy* **2021**, 21, 100776; c) L. Zhou, J. Rada, Y. Tian, Y. Han, Z. Lai, M. F. McCabe, Q. Gan, *Phys. Rev. Mater.* **2022**, 6, 090201.
- [26] L. Fan, W. Li, W. Jin, M. Orenstein, S. Fan, *Opt. Express* **2020**, 28, 25460.
- [27] N. Jaziri, A. Boughamora, J. Müller, B. Mezghani, F. Tounsi, M. Ismail, *Energy Rep.* **2020**, 6, 264.
- [28] M. A. Zaman, *Int. J. Therm. Sci.* **2019**, 144, 21.
- [29] H. A. Macleod, *Thin Film Optical Filters*, CRC Press, Boca Raton, FL **2010**.
- [30] a) S. Y. Jeong, C. Y. Tso, J. Ha, Y. M. Wong, C. Y. H. Chao, B. Huang, H. Qiu, *Renewable Energy* **2020**, 146, 44; b) Z. Chen, L. Zhu, A. Raman, S. Fan, *Nat. Commun.* **2016**, 7, 13729; c) M. A. Kecebas, M. P. Menguc, A. Kosar, K. Sendur, *J. Quant. Spectrosc. Radiat. Transfer* **2017**, 198, 179.
- [31] Gemini Observatory, *Atmospheric Transmission Data*, Gemini Observatory, Hilo, HI **2005**, <http://www.gemini.edu/sciops/observing-gemini>.
- [32] ASTM G173-03 Reference Spectra Derived from SMARTS v. 2.9.2, <https://www.nrel.gov/grid/solar-resource/renewable-resource-data.html>
- [33] E. D. Jackson, *Transactions of the Conference on the Use of Solar Energy*, University of Arizona Press, Tuscan, AZ **1955**.
- [34] a) A. Mojiri, R. Taylor, E. Thomsen, G. Rosengarten, *Renewable Sustainable Energy Rev.* **2013**, 28, 654; b) C. Stanley, A. Mojiri, G. Rosengarten, *Nanophotonics* **2016**, 5, 161; c) A. G. Imenes, D. R. Mills, *Sol. Energy Mater. Sol. Cells* **2004**, 84, 19.
- [35] D. Enescu, *Green Energy Advances*, IntechOpen, London **2019**.
- [36] G. Min, *Energy Environ. Sci.* **2022**, 15, 356.
- [37] K. Araki, Y. Ota, H. Saiki, H. Tawa, K. Nishioka, M. Yamaguchi, *Appl. Sci.* **2019**, 9, 4598.
- [38] P. Breeze, *Solar Power Generation*, Academic Press, London, UK **2016**.
- [39] F. Languy, S. Habraken, *Opt. Lett.* **2013**, 38, 1730.
- [40] J. R. Wilcox, Ph.D. Thesis, Purdue University, XX **2013**.
- [41] M. Planck, *The Theory of Heat Radiation*, Dover, New York **1914**.
- [42] L. C. Hirst, N. J. Ekins-Daukes, *Prog. Photovoltaics* **2011**, 19, 286.
- [43] M. Zeyghami, D. Y. Goswami, E. Stefanakos, *Sol. Energy Mater. Sol. Cells* **2018**, 178, 115.
- [44] H. Hashim, J. J. Bompfrey, G. Min, *Renewable Energy* **2016**, 87, 458.
- [45] F. Meillaud, A. Shah, C. Droz, E. Vallat-Sauvain, C. Miazza, *Sol. Energy Mater. Sol. Cells* **2006**, 90, 2952.
- [46] a) G. Min, *J. Electron. Mater.* **2010**, 39, 1782; b) D. M. Rowe, *CRC Handbook of Thermoelectrics*, CRC Press, London **2006**.
- [47] C. G. Granqvist, A. Hjortsberg, *J. Appl. Phys.* **1981**, 52, 4205.